

# High Temperature Corrosion Research at The Albany Research Center

Bernard S. Covino, Jr.

Albany Research Center, U. S. Department of Energy, 1450 Queen Avenue, S. W., Albany, OR 97321  
E-mail: [covino@alrc.doe.gov](mailto:covino@alrc.doe.gov); Telephone: (541) 967-5828; Fax: (541) 967-5914

Gordon R. Holcomb, James H. Russell, Stephen D. Cramer, Sophie J. Bullard, Margaret Ziomek-Moroz,  
Steven A. Matthes, and Richard E. Chinn

Albany Research Center, U. S. Department of Energy, 1450 Queen Avenue, S.W., Albany, OR 97321

## Manuscript

### Abstract

The Severe Environment Corrosion and Erosion Research Facility (SECERF) at the Albany Research Center is operational. SECERF consists of 6 modules that share the availability of up to 10 different gases to produce environments for high temperature corrosion and erosion research. Projects to be conducted in the modules include: corrosion sensors for fossil energy systems, thermal gradient effects on high temperature corrosion, the development of sulfidation resistant alloys, determination of the effects of ash on the corrosion of metals and alloys in coal and waste combustion and coal gasification environments, high temperature erosion-corrosion of metals, and molten slag effects on refractories. Results from two areas, the effect of ash deposits on alloy corrosion and thermal gradient effects on the corrosion of metals, will be highlighted.

Ash produced in coal gasifiers, coal combustors, and waste combustors, when deposited on metal surfaces, provides sites for corrosion attack and contributes chemical species that participate in the corrosion reaction. Results are presented for the corrosion of 304L stainless steel, that was either uncoated or coated with ash or with ash containing NaCl or Na<sub>2</sub>SO<sub>4</sub>, in air-water vapor mixtures at 600° C.

The presence of high heat fluxes and temperature gradients in many fossil energy systems creates the need for an understanding of their effects on corrosion and oxidation. Such information would be useful for both improved alloy design and for better translation of isothermal laboratory results to field use. Temperature gradients in a solid oxide result in two changes that modify diffusion within the oxide. The first is when a gradient in point defect concentration is created within the oxide, for example, where more vacancies are expected at a higher temperature. The second change is when the presence of a temperature gradient biases the diffusion jump of an atom. Results of tests are presented for cobalt with metal surface temperatures of approximately 920-950° C in N<sub>2</sub> plus 1-10 vol% O<sub>2</sub> environments with a heat flux of about 40 kW/m<sup>2</sup>. Non-equilibrium thermodynamics were used to develop oxidation rate equations in temperature gradients that were combined with point defect information of CoO to predict oxidation rates.

## **Introduction**

Reactors, gasifiers, pipelines, heat exchangers and many other power-generation structures in the 21st century require materials that can perform reliably in ever-increasing temperatures and pressures, for longer times, and in a variety of corrosive atmospheres. Economic and environmental concerns are the primary driving forces for improvements in the energy industries. One of the keys to development of materials that can meet these requirements is a laboratory that can be used to safely and reproducibly simulate the hostile environments of power generation.

The Severe Environment Corrosion and Erosion Research Facility (SECERF) has been established at the U.S. Department of Energy's Albany Research Center in Albany, Oregon, USA, to develop materials that can withstand the severe conditions of power generation and other high-temperature processes. SECERF has six specialized research modules, each featuring a furnace or reaction chamber, up to ten metered input gases, and an automated control and data acquisition system. An update of the capabilities, applications, and current research of each module are discussed here.

## **SECERF**

The nine metered gases available for researchers are CO, CO<sub>2</sub>, O<sub>2</sub>, CH<sub>4</sub>, H<sub>2</sub>, SO<sub>2</sub>, N<sub>2</sub>, H<sub>2</sub>S and HCl. One option for the tenth gas is to use different gases as research needs change. Each gas flows through a manual valve, a solenoid valve, a digital mass flow controller and a check valve. Four of the gases—O<sub>2</sub>, CH<sub>4</sub>, H<sub>2</sub> and CO—flow through a flashback arrester. Water vapor can be added using a metering pump and a heated section of tubing. Air and cooling water are also available for control of experimental apparatus parameters. Digital gas leak detectors are strategically placed in each module, the surrounding room, and the gas shed. Detectors are connected to audible and visible alarms that are located both inside and outside of the SECERF. All the metered gases are dispensed from cylinders securely stored in a gas shed, where the cylinders can be changed from outside the building. The detectors and alarms are connected to the solenoid valves, such that the gases can be automatically shut off and the lines flushed with N<sub>2</sub> in the event of a leak or fire.

## **Module 1 - Gas Transmission Pipelines**

A commercially-available field-ready electrochemical noise (ECN) corrosion sensor system is being evaluated for use in and around gas transmission pipelines. The ECN sensors are being used to study the effect of salt, O<sub>2</sub>, and CO<sub>2</sub> concentrations at room temperature on the water corrosion of pipeline steel. ECN sensors are also being evaluated in soil environments typical of the exterior of gas transmission pipelines. The final phase of the research will investigate ECN sensor design and operation in low pressure simulated gas transmission pipeline environments consisting of CH<sub>4</sub>, CO<sub>2</sub> and H<sub>2</sub>O.

## **Module 2 - Thermal Gradient Effects**

The effects of thermal gradients and heat flux on protective metal oxide scales in high-temperature oxidizing environments are studied in the second module. Samples are air-cooled on one side and exposed to an oxygen-nitrogen atmosphere on the other side, as shown in the tube furnace insert in Fig.

1. Heat fluxes can reach 40 to 50 kW/m<sup>2</sup>, as compared to 400 kW/m<sup>2</sup> in evaporator tube walls and 200 kW/m<sup>2</sup> in superheater tube walls.[1]

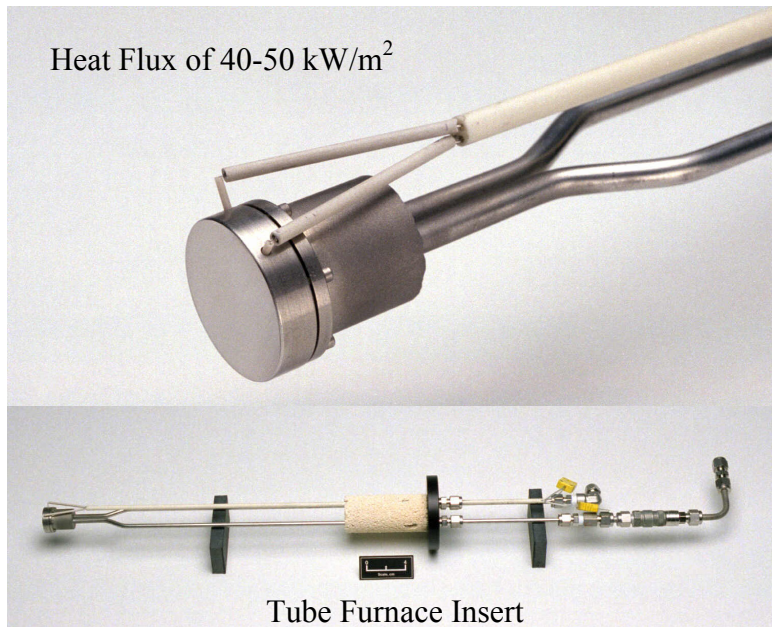


Fig. 1: Tube furnace insert for one-sided cooling of sample with compressed air. The assembly includes a 25 mm diameter machined cobalt disc with internal thermocouples.

biases the jumps. This transport of heat is described by the heat of transport,  $Q^*$ , and is the heat carried from the initial site to the final site.[1]

Both Glover [2] and Malik [3-4] have used non-equilibrium thermodynamics [5] to develop general flux equations that can be combined with point defect information of specific oxides to predict oxidation rates. The general flux equation, from Malik [3-4] is

$$J_i = -\frac{Nc_iD_i}{kT} \left\{ \left(1-t_i\right) \left[ \frac{d\mu_i}{dx} + \frac{Q_i^*dT}{Tdx} \right] - q_i \sum_{k \neq i} \frac{t_k}{q_k} \left( \frac{d\mu_k}{dx} + \frac{Q_k^*dT}{Tdx} \right) \right\} \quad (1)$$

Where  $J_i$  is the flux of species  $i$  in the oxide,  $N$  is the number of lattice sites available to species  $i$  per unit volume,  $c_i$  is the concentration of species  $i$ ,  $D_i$  is the diffusion coefficient of species  $i$ ,  $k$  is Boltzmann's constant,  $T$  is temperature,  $t_i$  is the transport number of species  $i$ ,  $\mu_i$  is the chemical potential of species  $i$ ,  $x$  is the distance into the oxide from the metal, and  $q_i$  is the effective charge of species  $i$ . Equation 1 differs from Glover [2] by including the consequences of effective charge on the

Heat flux effects can change the oxidation process in two basic ways: from thermal stress effects and from diffusion effects. Experiments with the oxidation of cobalt to CoO attempt to verify predictions of changes in point defect diffusion in CoO in a temperature gradient.

Temperature gradients in a solid oxide result in two changes that modify diffusion within the oxide. The first is when equilibrium concentrations of point defects are a function of temperature. A gradient in point defect concentration can be created within the oxide, for example, in the case where more vacancies are expected at higher temperature. The second change is associated with the heat carried with each diffusion jump of an atom. Since each jump results in a transport of heat, the presence of a temperature gradient

---

<sup>[1]</sup>A similar term found in the literature is the reduced heat of transport,  $Q^{*'}$ , and is the portion of  $Q^*$  in excess of the partial molar enthalpy,  $h$ . Thus  $Q^{*'} = Q^* - h$ .

diffusion process ( $t_i$  and the  $q_i \Sigma(\cdot)$  term). When the temperature gradient is zero and neglecting any effects of effective charge, then Equation 1 simplifies to Fick's first law of diffusion.

Equation 1 can be solved [6] and compared to experimental results in terms of oxide thickness measurements as a function of time. An example of oxide thickness measurements after exposure to 10 vol% O<sub>2</sub> at 1100°C for 18 minutes with a heat flux of 20 kW/m<sup>2</sup> is shown in Fig. 2.

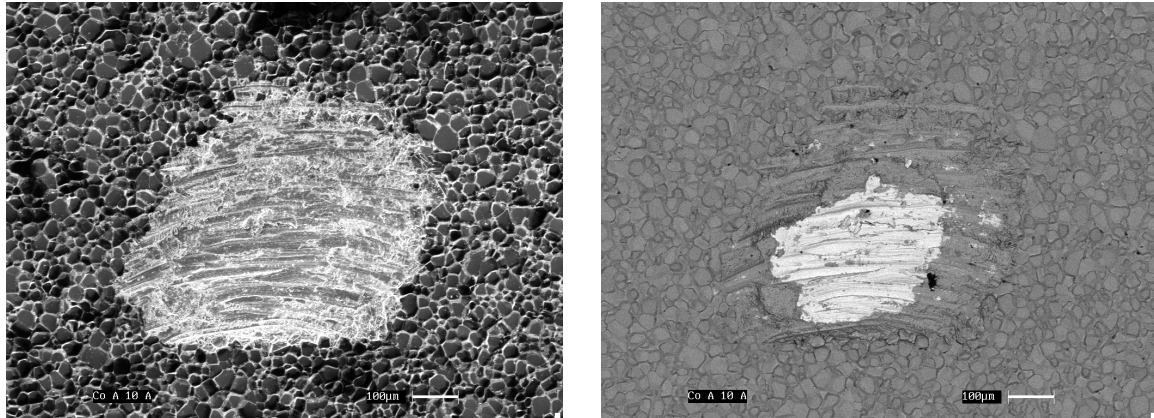


Fig. 2: Secondary electron (left) and backscattered electron (right) images of a CoO scale formed on Co after exposure to 10 vol% O<sub>2</sub> at 1100°C for 18 minutes with a heat flux of 20 kW/m<sup>2</sup>. The nicks were made with a drill bit at an angle of 45 degrees. The scale thickness was 150±20  $\mu\text{m}$ .

### Module 3 - Sulidation-Resistant Alloys

Iron-based alloys that are used in energy conversion processes with sulfidizing environments are tested in the third module. Of particular interest are the effects of aluminum and silicon in stainless steels

between 500 and 800°C. Results of this research are contained in the paper, "Improved Austenitic Steels for Power Plant Applications" by D. E. Alman, J. S. Dunning, K. K. Schrems, J. C. Rawers, R. W. Wilson, J. A. Hawk, and A. V. Petty, Jr., published as part of the 16<sup>th</sup> Fossil Energy Materials Conference Proceedings.



Figure 3: The photo shows the tube furnace and equipment that is used in Module 4

Figure 3. An additional apparatus is in design to evaluate the effects of molten chloride and sulfate salts on the corrosion and electrochemistry of alloys.

### Module 4 - Ash-Covered Alloy Corrosion

The fourth module has multiple purposes. The effects of ash coatings on the corrosion of materials in coal combustion, coal gasification and waste-to-energy environments will be studied in the apparatus shown in

Research has been initiated to study the effect of ash and modified ash on the corrosion of 304L stainless steel. The composition of the ash, which was obtained from a coal gasification process, is listed in Table 1. The ash was used as is or modified by adding either 5% (by weight)  $\text{Na}_2\text{SO}_4$  or 5%  $\text{NaCl}$ .

Table 1: Composition of gasifier ash used in corrosion research

Composition, weight %					
O = 26.7	C = 22.0	Al = 5.71	Ca = 2.08	Cr = 0.012	Cu = 0.012
Fe = 13.6	K = 1.12	Hg < 0.1	Mg = 0.36	Mn = 0.021	Mo = 0.008
N = 0.68	Na = 1.39	Ni = 0.009	P = 0.053	Pb = 0.007	S = 1.7
Si = 13.1	Sn = <0.01	Ti = 0.18	V = 0.012	Zn = 0.017	

304L SS samples were coated on one side with a water-based slurry of either the ash or the modified ash and allowed to air dry for 14 hours prior to starting the experiment. Samples were mounted horizontally with the ash-coated side facing up, and positioned on small sections of glass tubing resting inside an alumina tray. The alumina trays plus samples were positioned within the constant temperature zone of the tube furnace, heated to 600°C under a nitrogen flow, and then switched to an air-12 vol% water mixture when at temperature. Two of each type of samples were exposed for 5 days (120 h) and then allowed to cool to room temperature under a flow of nitrogen. A picture of the samples sitting on the alumina trays after removal from the experiment is shown in Figure 4.



Figure 4: Samples after removal from the experiment. From left to right: ash +  $\text{NaCl}$ , ash +  $\text{Na}_2\text{SO}_4$ , ash, uncoated, ash +  $\text{NaCl}$ , uncoated, ash +  $\text{Na}_2\text{SO}_4$ , and ash. Sample size: 1" X 1".

After removal from the tube furnace, one of each type of samples was cleaned using water and mild scrubbing. No chemical stripping of adherent oxide films has been conducted yet. Gravimetric corrosion rates were determined by measuring the weight loss of these samples. The remaining one of each type of sample was submitted for cross sectioning, polishing, and metallographic analysis. Analysis of the corroded layer revealed some interesting differences based on the presence of ash and/or the salts. Figure 5 shows photomicrographs of the cross sections of samples of each type.

All of the photos show evidence of the beginning of grain boundary attack. The addition of ash and the modified ashes cause increased attack of the metal surface that follows the order: uncoated < ash < ash +  $\text{Na}_2\text{SO}_4$  < ash +  $\text{NaCl}$ . The attack in the  $\text{NaCl}$  modified ash resembles pitting.

Worst-case sample thickness values were obtained also from the metallographic examination. These are worst case values because they were measured using the point of deepest penetration observed in the cross section, and not an average value for the entire surface. These were compared to initial sample thickness measured using a digital micrometer prior to insertion into the experiment. The thickness

changes measured here were converted into a penetration rate and are reported in Table 2 and compared to gravimetric penetration rates.

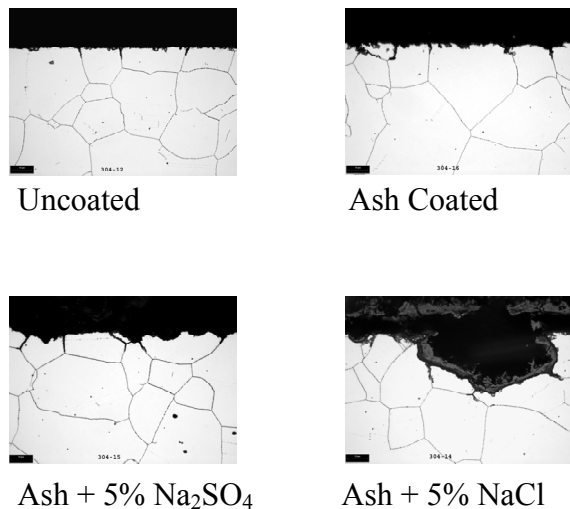


Figure 5: Photomicrographs of cross sections of 304L SS samples either uncoated or coated with ash or modified ash and exposed at 600°C to air + 12% H<sub>2</sub>O for 5 days (scale marker: 10 μm).

Table 2: Comparison of penetration rates for 304L SS determined by gravimetric and by thickness change measurements.

Penetration rates, μm/y		
Sample Type	Gravimetric	Thickness Change
Uncoated	62.5	612
Ash	75.8	1057
Ash + Na <sub>2</sub> SO <sub>4</sub>	128.2	927
Ash + NaCl	418.7	6489

The order of corrosion attack by the ash and modified ashes, shown in Table 2, is exactly the same as observed visually in Figure 5. That is, the presence of ash and salts such as NaCl and Na<sub>2</sub>SO<sub>4</sub> greatly accelerate the corrosion of 304L SS, with NaCl having the greatest effect. There are significant differences between the penetration rates measured either gravimetrically or by thickness changes.

There are several reasons why penetration rates measured by thickness change are as much as an order of magnitude greater than gravimetric penetration rates. One reason is that worst case thickness changes were used. Another is the statistical nature of sampling the surface at the point where the cross section was taken. A cross section in another area could give significantly different thickness changes. There are also more errors built into the initial and final thickness measurements than the gravimetric

measurements. Measurement of initial sample thickness gave standard deviations ranging from 0.25 to 5.3 micrometers. Finally, measurement of the final thickness from the cross-sections relies on the sample cross sections being mounted as close to perpendicular as possible.

The mounted and polished cross sections were also examined on the analytical scanning electron microscope (ASEM) to gain insight into the mechanism of corrosion attack. The ASEM includes examination of corroded cross sections using backscattered electron imaging (BSE) to detect atomic number changes at the scale alloy interface, energy dispersive spectroscopy (EDS) for element x-ray maps and line scans, and wavelength dispersive spectroscopy (WDS) for line scans. Results for the samples discussed above were not complete at the time this paper was prepared, but results for samples exposed to the same environment at 500°C are available and will be discussed here to show some trends in this research.

X-ray maps for Fe, Cr, Ni, and S for samples coated with ash and ash + NaCl will be discussed in terms of the effect of NaCl. NaCl causes the growth of a much thicker corrosion product which has a distinct layer of iron-, nickel-, and sulfur-rich compounds at the outer layer of the corrosion product. Without NaCl, these corrosion product layers are much closer to the metal surface and seem to be more protective of that surface. The sulfur in the corrosion product is contributed by the ash.

## Module 5 - High-Temperature Metal Erosion

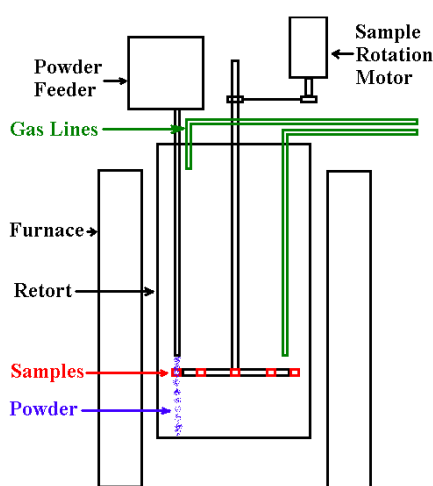


Figure 6: Schematic of the furnace for high-temperature erosion. Abrasive particles are fed from the upper left at a known rate onto the rotating sample rack.

Alloy coupons mounted on a rotating rack inside a furnace are abraded by a stream of quartz sand, in the fifth module. The temperature range of planned research is 350–600°C in reducing conditions, and 600–900°C in an oxidizing atmosphere. The reducing atmosphere includes H<sub>2</sub>S and HCl gases to simulate a gasifier, while the oxidizing atmosphere includes SO<sub>2</sub> and HCl at 1 atm pressure to simulate a combustor. The 20–250 µm diameter abrasive particles flow at a velocity of 10–40 m/s and a flux of 0.1–1 mg cm<sup>-2</sup> s<sup>-1</sup>. A typical test duration is 50–100 hours.

The test simulates the abrasive conditions in the convective heat transfer regions inside a boiler in a fossil energy plant. The particle velocity can be decreased to simulate a fluidized bed, or increased to simulate the abrasion experienced by a turbine. The apparatus is shown schematically in Figure 6.

## Module 6 - Gasifier Refractories



**Figure 7a:** Furnace and cart for dripping molten slag on a test refractory brick. The spent slag is collected in the black barrel below the cart. The slag feed tube protrudes from the front of the upper part of the furnace. The slag feeder is not shown.

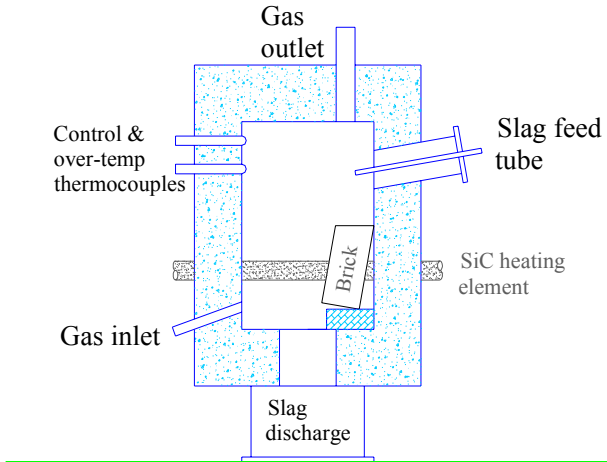


**Figure 7b:** Schematic of the furnace in Figure 6a. The sight tubes, slag feeder, and additional thermocouples and heating elements are not shown.

Inclined refractory bricks are subjected to a stream of dripping slag in the sixth module, according to ASTM C768. The powdered slag is fed from a hopper above the furnace in Figure 7a by a water-cooled auger at a constant rate, about 8 kg/hr. The slag particles melt as they fall onto the test brick inside the 1600°C furnace. The bricks are machined to create a basin drained by a groove. The molten slag falls into the basin at the high end of the brick, flows down the central groove, and off the brick, as shown in Figure 7b. The initial impingement has an erosive effect. The molten slag diffuses into and reacts with the refractory while it flows. The slag's viscosity increases as the slag cools and leaves the brick. An auxiliary heater keeps the spent slag hot enough to remain fluid until it is discharged into a barrel below the furnace. The slag inlet and outlet are sealed to prevent the furnace gases, including H<sub>2</sub> and CO, from escaping into the module.

The purpose of the slag-drip apparatus is to evaluate the performance of refractory materials, both novel and established, as candidates for integrated combined-cycle gasifier linings.

## Conclusions

- The SECERF is operational and the modules are now being used to conduct high temperature corrosion and erosion research on metals and refractories.
- Corrosion of ash-coated alloys has been initiated and results show the effect of ash contaminants on corrosion attack.
- NaCl is more detrimental than Na<sub>2</sub>SO<sub>4</sub> to the corrosion of 304L SS in air-water environment at 600°C.

- NaCl impurities in ash tend to produce a thicker corrosion product that differs in the distribution of Fe, Cr, Ni, and S.
- Experiments with the oxidation of cobalt to CoO are being used to verify predictions of changes in point defect diffusion in CoO in a temperature gradient

## References

1. A. J. B. Cutler and E. Raask, "External Corrosion in Coal-Fired Boilers: Assessment from Laboratory Data," *Corrosion Science* 21 (1981) pp. 789-800.
2. D. M. Glover, "Heat Flux Effects on Oxidation Rates and Kinetics," *Corrosion Science* 20 (1980) pp. 1185-1193.
3. S. Malik, "Oxidation of Metals in a Temperature Gradient," Ph.D. Thesis, University of Kent at Canterbury (1990).
4. S. Malik and A. V. Chadwick, "Oxidation in a Temperature Gradient," *Microscopy of Oxidation*, (Institute of Metals, 1991) pp. 336-341.
5. R. E. Howard and A. B. Lidiard, "Matter Transport in Solids," *Reports on Progress in Physics* 27 (1964) pp. 161-240.
6. G. R. Holcomb, B. S. Covino, Jr., and J. H. Russell "Oxidation in a Temperature Gradient," *Proceedings of the 15<sup>th</sup> Annual Conference on Fossil Energy Materials*, (Oak Ridge National Laboratory, 2001).